

Adhesive Hybrid Interpenetrating Network Hydrogel-Based Detector to Monitor Solar Radiation Dose Required for Plant Growth

Neng Hu, Lei Shi, Shangchao Ji, Weijia Wang,* Lin Lei, Huiqing Fan, Peter Müller-Buschbaum,* and Qi Zhong*

An adhesive and visualized hydrogel-based detector is designed to monitor the solar radiation dose required for plant growth by the discoloration of methylene blue (MB) under sunshine. The detector is based on hybrid hydrogels prepared from photoinitiated polymerization. The combination of polypropylene (PP) fabrics acting as a substrate and the photoinitiated polymerization on the graphitic carbon nitride (g-C₃N₄) surface enables a smaller thickness and a more homogenous distribution of the g-C₃N₄ nanosheets. Thus, the hybrid interpenetrating network (IPN) hydrogel on the PP fabrics with a thickness of 1.5 mm presents an improved photodegradation capability. In addition, better mechanical properties and lower weight of the hydrogel-based detector are achieved by the presence of the PP fabrics. In combination with the stickiness from a polyurethane resin acting as glue, the obtained detector can be easily pasted on the leaf of a plant as demonstrated for the example of *Epipremnum aureum*. The radiation dose exposed to the leaves can be accurately traced from the change in color of the detector to ensure a sufficient radiation for plant growth and avoid possible burn to the leaves under sunshine.

can repair plant DNA by enzyme photolyase and favor the synthesis of chlorophyll in plants, which is indispensable for plants to perform photosynthesis.^[7] When exposed to solar radiation, the chlorophyll in plants might switch carbon dioxide (CO₂) and water (H₂O) to oxygen (O₂) and organic nutrients by photosynthesis, which is detrimental to plant growth.^[8–10] However, long-term overexposure to solar radiation has a side effect on plant growth. Excessive solar radiation may damage proteins, DNA, and cells in plants.^[11–13] This damage directly affects seed production, plant biomass, and growth as well as morphology.^[14,15] Thus, a real-time monitoring of the solar radiation dose, which plants are exposed to, has received growing interest. This holds in particular for shade-tolerant plants, which have strict requirements for sunshine conditions such as light intensity and time. It is also of high interest to modern in-door farming approaches, which are

based on the use of artificial illumination such as vertical farming.

In the case of human beings, internal and external stimuli can be directly measured by physiological signal changes such as body temperature, heart rate, and blood sugar. In contrast, the expression of plants, which involves subtle and slow changes, is not so prominent.^[16] For this reason,

1. Introduction

Solar radiation is the energy source that regulates ecological and physiological processes in plant ecosystems.^[1–5] Among the environmental factors such as moisture and soil fertility, solar radiation is the most influential one.^[6] Suitable solar radiation dose

N. Hu, Q. Zhong
Key Laboratory of Advanced Textile Materials & Manufacturing Technology
Ministry of Education
Zhejiang Sci-Tech University
Hangzhou 310018, China
E-mail: qi.zhong@zstu.edu.cn

L. Shi, S. Ji
Zhejiang Hexin Science and Technology Co., Ltd.
1568 Dongfang Road, Jiaxing 314003, China

 The ORCID identification number(s) for the author(s) of this article can be found under <https://doi.org/10.1002/adem.202201118>.

© 2022 The Authors. Advanced Engineering Materials published by Wiley-VCH GmbH. This is an open access article under the terms of the Creative Commons Attribution-NonCommercial License, which permits use, distribution and reproduction in any medium, provided the original work is properly cited and is not used for commercial purposes.

DOI: 10.1002/adem.202201118

W. Wang, L. Lei, H. Fan
State Key Laboratory of Solidification Processing
School of Materials Science and Engineering
Northwestern Polytechnical University
Xi'an 710072, China
E-mail: weijia.wang@nwpu.edu.cn

P. Müller-Buschbaum, Q. Zhong
Technische Universität München
Physik-Department
Lehrstuhl für Funktionelle Materialien
James-Frank-Str. 1, 85748 Garching, Germany
E-mail: muellerb@ph.tum.de

P. Müller-Buschbaum
Heinz Maier-Leibnitz Zentrum (MLZ)
Technische Universität München
Lichtenbergstr. 1, 85748 Garching, Germany

long-term and continuous monitoring are highly desired and demanded. At present, Lan et al. developed an on-plant self-powered sustainable agriculture system based on a breathable and waterproof triboelectric nanogenerator (WB-TENG).^[17] The constructed “intelligent agriculture” systems can convert environmental energy such as wind and raindrops into electricity and realize real-time monitoring of the health status of plants such as soil moisture, soil fertility, light intensity, and temperature by connecting with the Internet of Things (IoT). However, the specific information about solar radiation dose required for plant growth is still missing in such approach. Given the damage to plants induced by overexposure to solar radiation, it would become a main challenge in tracing the health status of plants in case systems like WB-TENG or alternatives are in operation. Alternatively, a photometer indeed can measure and quantify the light intensity more rapidly and accurately with a specific value.^[18] However, the photometer can only show the real-time intensity of the solar radiation. Due to the fact that the possible damage to plants is caused by the total dose of solar radiation, not the instant intensity, but the information about the dose is more crucial for plant cultivation. Especially on a cloudy day, when the solar intensity is changing with time, it will be very difficult to evaluate the dose with a photometer. In contrast, our presented hybrid hydrogel-based solar detector can visualize the dose by simply checking the color of the hybrid hydrogel. Therefore, the total dose of solar radiation exposed to a plant can be obtained in a simple manner, which is of great importance for plant growing. In addition, a photometer would require an external power supply and cannot be pasted on plant leaves to monitor the solar radiation because of its large size and heavy mass. This obviously hinders the application of conventional photometers to monitor the dose of solar radiation required for plant growth.

In such context, cheap and simple detectors for solar radiation dose, which could be adhered onto, e.g., plant leaves, appear very interesting.

As a metal-free photocatalytic material, graphitic carbon nitride (g-C₃N₄) has attracted intensive interest due to its low production costs, moderate bandgap, proper band position as well as physical and chemical stability.^[19–24] However, similar to graphene, g-C₃N₄ still suffers from certain drawbacks, such as easy aggregation in solvents and difficult recyclability.^[25,26] Thus, it is of great importance to establish an ideal supporting substrate for g-C₃N₄ nanosheets with better distribution and cyclability, which will extend the application of g-C₃N₄ nanosheets to monitor solar radiation required for plant growth. Hydrogels are polymers with a 3D network structure and have the characteristics of water absorption, moisturizing, and good softness.^[27–29] Thus, hydrogels have been broadly investigated and applied in the fields of drug delivery,^[30] tissue engineering,^[31] photocatalysis,^[32] and smart textiles.^[33] In our previous investigations, g-C₃N₄ was introduced into thermoresponsive hydrogels to realize good support for the photocatalyst g-C₃N₄. To overcome the drawback of poor mechanical properties, an interpenetrating network (IPN) structure was established in the hydrogels as well. However, still some drawbacks remained. For instance, due to the structure of the g-C₃N₄ nanosheets, they tend to aggregate and form large clusters in the hybrid IPN hydrogels. The presence of such large clusters strongly reduces the photodegradation efficiency. Besides that, the mechanical properties and weight were not

optimal. Due to the possession of a large amount of water, the hydrogels were soft and lack mechanical strength. Therefore, the hydrogels needed have a certain thickness, usually in the centimeter scale, to maintain their shape unchanged during the application. Although the mechanical properties were improved, the weight of the hydrogels was significantly increased, which prevents them to become suitable candidates for applications requiring low weight, such as detectors located on plant leaves. Thus, to simultaneously enhance the photodegradation efficiency and reduce the weight of the detector, a new approach of preparing hybrid IPN hydrogels is highly desired for the use as a solar radiation detector for monitoring plant growth.

In the present investigation, polypropylene (PP) fabrics are introduced into hybrid IPN hydrogels. Due to the flexibility and strength of the PP fabrics, the hybrid IPN hydrogels on this flexible supporting substrate can be much thinner without sacrificing mechanical integrity. Therefore, the obtained hybrid IPN hydrogels on PP fabrics are able to present excellent mechanics and flexibility simultaneously. In contrast, using an adhesive instead of the PP fabrics cannot improve the strength of the hybrid IPN hydrogels. For this reason, they will be easily damaged not only in the application, but also during the transport and storage. Thus, instead of an adhesive, PP fabrics are more suitable as substrate of the hybrid IPN hydrogels in the present investigation. The photodegradation efficiency of a dye can be prominently improved in such an approach. Moreover, by simply adding methylene blue (MB) during preparation, the hybrid IPN hydrogel on the PP fabrics can be used as the solar radiation detector, which visualizes the radiation dose by the discoloration of the MB. After being immersed in a polyurethane resin, such detector can be adhered onto plant leaves. After an initial calibration, the obtained detector can accurately monitor the solar radiation dose to avoid the possible burn of the plants by checking the discoloration of the detector under sunshine. The detector function is demonstrated for the example of the shade-tolerant plant *Epipremnum aureum*.

2. Results and Discussion

2.1. Structure and Morphology of Hybrid IPN Hydrogels on PP Fabrics

The functional groups in the hybrid IPN hydrogel on PP fabrics are probed by attenuated total reflection Fourier transform infrared (ATR-FTIR) spectroscopy. The characteristic absorption peaks of the triazine unit and its ring skeleton from g-C₃N₄ nanosheets (green curve in **Figure 1**) are observed at 810 and 1200–1620 cm⁻¹, respectively. A prominent absorption peak at 3000–3300 cm⁻¹ is observed as well, which is mainly attributed to the stretching vibration of N–H in g-C₃N₄ nanosheets.^[34] In the spectra of the PP fabrics (purple curve in **Figure 1**), the characteristic absorption peaks corresponding to C–C, –CH₂, and –CH₃ are visible at 1300–1500, 2837, and 2900–3000 cm⁻¹, respectively.^[35] Obviously, all these above characteristic absorption peaks from g-C₃N₄ nanosheets and PP fabrics can be also observed in the spectra of hybrid IPN hydrogel on PP fabrics (red curve in **Figure 1**) as well. It demonstrates that

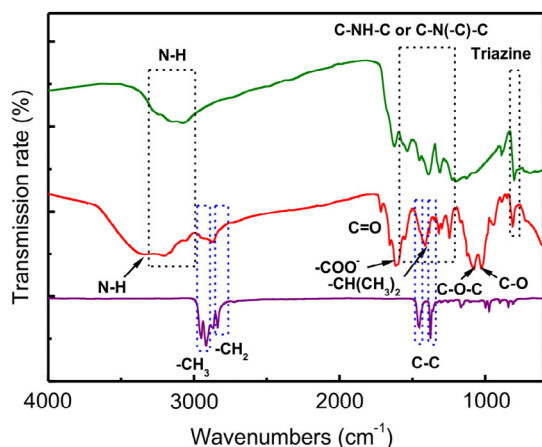


Figure 1. ATR-FTIR spectra of g-C₃N₄ nanosheets (green curve), PP fabrics (purple curve), and hybrid alginate-Ca²⁺/P(NM-co-O₃₀₀)/g-C₃N₄ IPN hydrogel on PP fabrics (red curve).

g-C₃N₄ nanosheets and PP fabrics are successfully incorporated into the IPN hydrogel. In addition, the characteristic absorption peaks related to -COO- and C-O in the alginate-Ca²⁺ component are found at 1615 and 1026 cm⁻¹, respectively.^[36,37] The absorption peaks of N-H, -CH(CH₃)₂, and C=O in the PNM component can be seen at 3200–3500, 1412, and 1716 cm⁻¹, respectively.^[38,39] The absorption peak at 1110 cm⁻¹ is the stretching vibration peak of C-O-C in the PO₃₀₀ component.^[40] The structure of the hybrid hydrogels is composed of physical cross-linking formed by alginate-Ca²⁺ and chemical cross-linking formed by P(NM-co-O₃₀₀)-MBA. The two cross-linking systems interpenetrate to each other and form an IPN structure. In our previous investigation, the mechanical properties of pure P(MEO₂MA-co-OEGMA₃₀₀) hydrogels with single chemical cross-linking and alginate-Ca²⁺/P(MEO₂MA-co-OEGMA₃₀₀) IPN hydrogels with both chemical and physical cross-linking were investigated.^[41] We demonstrated that the mechanical properties were significantly improved after introduction of physical cross-linking and the formation of the IPN structure. Because the IPN structure is profoundly influenced by the extent of interpenetration of the chemical and physical cross-linking systems, it can be improved by optimizing the solubility and dispersibility of hydrogels before solidification. By comparing and analyzing the ATR-FTIR spectra of g-C₃N₄ nanosheets, PP fabrics, and hybrid alginate-Ca²⁺/P(NM-co-O₃₀₀)/g-C₃N₄ IPN hydrogel on PP fabrics, it can be concluded that the hybrid alginate-Ca²⁺/P(NM-co-O₃₀₀)/g-C₃N₄ IPN hydrogel is successfully prepared on the PP fabrics.

Because the supporting substrate and initiation approaches are strongly correlated to the structure of the hybrid hydrogel, the morphology of the PP fabrics and of the hybrid alginate-Ca²⁺/P(NM-co-O₃₀₀)/g-C₃N₄ IPN hydrogel on the PP fabrics is compared. **Figure 2a** presents the surface morphology of the PP fabrics. Unlike the fibers prepared by electrospinning, the present PP fibers are not homogenous in diameter (diameter varies between 1 and 5 μm). They are randomly distributed in the fabrics, which is mainly caused by the nonwoven preparation of the PP fabrics. The cross section of the hybrid IPN hydrogel on

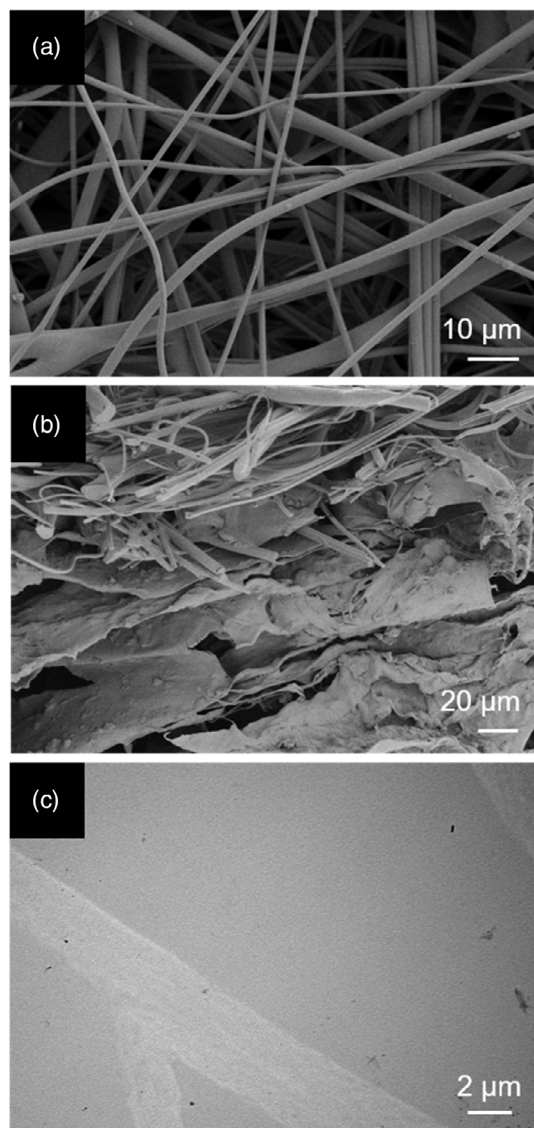


Figure 2. a) SEM image from the surface of the PP fabrics. b) SEM image from the cross section of hybrid IPN hydrogel on the PP fabrics. c) TEM image from the cross section of hybrid alginate-Ca²⁺/P(NM-co-O₃₀₀)/g-C₃N₄ IPN hydrogel on the PP fabrics.

the PP fabrics is presented in Figure 2b. Obviously, the upper part is the PP fabrics whereas the bottom part is the hybrid IPN hydrogel. Moreover, a huge number of pores with a size of 30 μm are found in the hybrid IPN hydrogel. This porous structure can profoundly promote the diffusion of MB into the hydrogel. Plenty of small particles are visible in the hybrid IPN hydrogels, which are attributed to the g-C₃N₄ nanosheets. In combination with the homogenous distribution of g-C₃N₄ nanosheets in the hybrid IPN hydrogel co-initiated by g-C₃N₄ and triethylamine (Figure 2b), improved adsorption and photodegradation of MB are expected.^[34] To address the distribution of g-C₃N₄ in the hybrid IPN hydrogel on the PP fabrics, transmission electron microscopy (TEM) images of the hybrid IPN hydrogel on the PP fabrics are presented in Figure 2c. In our previous investigation about hybrid IPN hydrogels, besides scanning

electron microscopy (SEM) and TEM, the distribution of g-C₃N₄ nanosheets in the hybrid IPN hydrogels was further explored by MB removal measurements.^[40] Compared to the hybrid hydrogels initiated by APS/TEMED, the MB removal of hybrid hydrogels photoinitiated by g-C₃N₄/triethylamine was significantly faster. More than 80% MB was removed in 5 h, which was 30% faster than that in the hybrid hydrogels initiated by APS/TEMED. This profound improvement was caused by the homogeneity of the g-C₃N₄ nanosheets formed by the photoinitiated polymerization of hybrid hydrogels. It indeed reduced the aggregation of g-C₃N₄ nanosheets and enhanced the photodegradation performance. Because the polymerization sets in on the g-C₃N₄ surface, the aggregation of g-C₃N₄ is efficiently hindered. It results in a higher specific surface area of g-C₃N₄ in the hydrogel, which is favorable for the photodegradation of dyes under radiation.

2.2. Photodegradation Capability of Hybrid IPN Hydrogels on PP Fabrics

PP fabrics not only possess stable physical and chemical properties, but also show good flexibility, which renders them well suitable as supporting substrates for the hybrid IPN hydrogels.^[42–44] Moreover, with the support of the PP fabrics, the thickness of the hybrid IPN hydrogel can be significantly reduced, which reduces the weight of the hybrid hydrogel and favors low weight applications. To demonstrate this positive impact, three hybrid IPN hydrogels on PP fabrics are prepared with different thicknesses (1.5, 3, and 6 mm). In case of the hybrid IPN hydrogel on the PP fabrics with a thickness of 6 mm, the MB removal rate is only 22% in the first half hour (black curve in Figure 3a). Further prolonging the time, it can reach 100% in 12 h. When the thickness is reduced to 3 mm, the MB removal rate in the first half-hour is significantly increased to 35% (orange curve in Figure 3a), which is almost doubled to that with a thickness of 6 mm. In addition, the removal of MB can be finished in 8 h, which is also 50% faster. The faster process is caused by the larger surface area of the thinner IPN hybrid hydrogel on the PP fabrics. Because the total amount of hydrogel on the PP fabrics is the same, the reduction of the layer thickness significantly increases the surface area, which is beneficial for the adsorption of MB. With a reduction of the thickness to 1.5 mm, the removal rate again increases to 58.0 ± 0.1% (red curve in Figure 3a), which is almost 3 times to that of the thickness of 6 mm. Already after 3 h, almost all MB is removed from the aqueous solution. Thus, it can be concluded that due to the support of the flexible PP fabrics, the thickness of hybrid IPN hydrogels can be significantly reduced to realize a large surface area and excellent photodegradation of MB. Moreover, the lighter weight of the hybrid IPN hydrogel with a lower thickness favors a use in low weight applications. In addition, the kinetics can provide further information related to the degradation of MB. Thus, the degradation kinetics of MB by the g-C₃N₄ nanosheets and the hybrid IPN hydrogel on the PP fabrics are further investigated. As shown in Figure S1a, Supporting Information, in case of g-C₃N₄ nanosheets (purple), the MB degradation rate is higher at the beginning, which is related to the availability of active sites on g-C₃N₄ nanosheets. Because the number of dye molecules and active sites is reduced

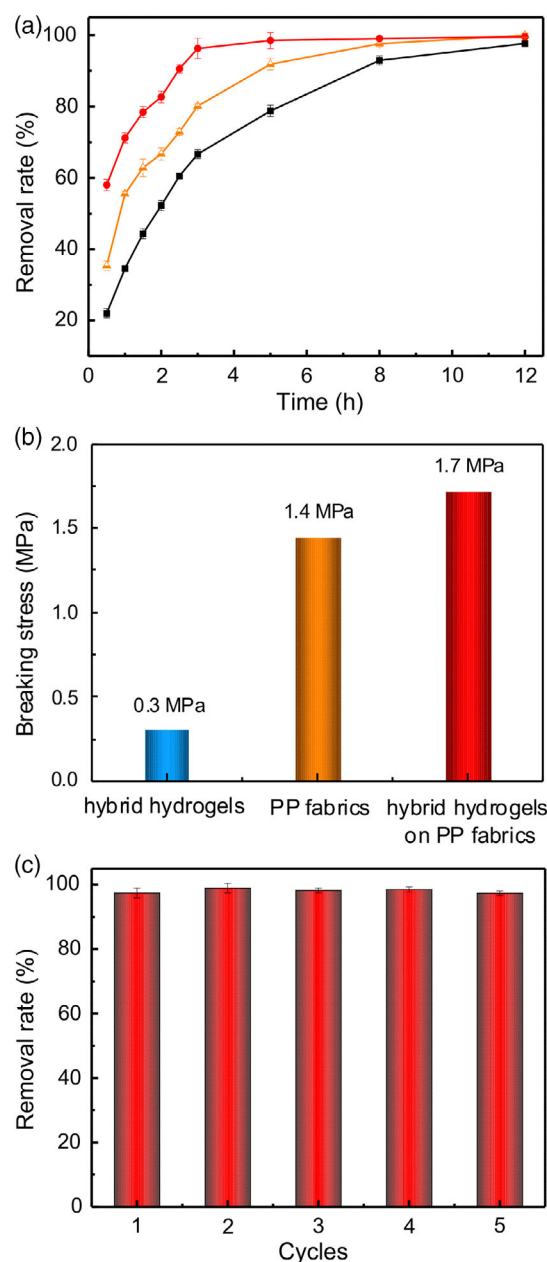


Figure 3. a) MB removal in the hybrid alginate-Ca²⁺/P(NM-co-O₃₀₀)/g-C₃N₄ IPN hydrogel on the PP fabrics with different thicknesses (red 1.5 mm, orange 3 mm, and black 6 mm). b) The breaking stresses of the pure hybrid P(NM-co-O₃₀₀)/g-C₃N₄ IPN hydrogel (blue), PP fabrics (orange), and the hybrid P(NM-co-O₃₀₀)/g-C₃N₄ IPN hydrogel on the PP fabrics (red) at broken tensile strain (33%). c) MB removal by hybrid IPN hydrogel on the PP fabrics in five consecutive adsorption and photodegradation cycles with 5 h per cycle light radiation.

during the photodegradation process, the removal rate is slightly reduced after 0.5 h. However, the removal rate remains constant based on the photodegradation mechanism. In case of the hybrid IPN hydrogel on the PP fabrics (orange), the removal of MB consists of two processes: one process is the adsorption of MB by the hydrogels and the second process is the degradation of MB by the

$g\text{-C}_3\text{N}_4$ nanosheets. Both processes take place simultaneously, which can enhance the removal rate of MB by the hybrid IPN hydrogel on the PP fabrics. Thus, the degradation of MB is faster during the first 0.5 h. After that, it is slower with time. The linear fit shown in Figure S1b,c, Supporting Information, demonstrates that the degradation of MB by the $g\text{-C}_3\text{N}_4$ nanosheets and the hybrid IPN hydrogel on the PP fabrics follows the pseudo-first-order kinetics and pseudo-second-order kinetics, respectively. The degradation kinetics illustrates that the hybrid IPN hydrogel on the PP fabrics possesses excellent degradation properties. As shown in Figure 3c, there is no prominent change of the MB removal in five consecutive cycles.

The optimized concentration of $g\text{-C}_3\text{N}_4$ nanosheets in the hybrid IPN hydrogel on the PP fabrics is studied by the MB removal measurements containing different amounts of $g\text{-C}_3\text{N}_4$ nanosheets in the hybrid alginate- $\text{Ca}^{2+}/\text{P}(\text{NM-co-O}_{300})/g\text{-C}_3\text{N}_4$ IPN hydrogel on the PP fabrics. After 8 h, almost all MB is removed by the hybrid IPN hydrogel on the PP fabrics containing 20 mg $g\text{-C}_3\text{N}_4$ nanosheets (purple curve in Figure S2, Supporting Information). When the amount of $g\text{-C}_3\text{N}_4$ nanosheets is increased to 50 mg (red curve in Figure S2, Supporting Information), the MB removal rate of the hybrid IPN hydrogel on the PP fabrics is profoundly improved. It only takes 5 h to reach the complete removal of MB. Thus, the removal efficiency is 1.6 times than that of the hybrid IPN hydrogel on the PP fabrics containing 20 mg $g\text{-C}_3\text{N}_4$ nanosheets. When further increasing the amount of $g\text{-C}_3\text{N}_4$ nanosheets to 80 mg (blue curve in Figure S2, Supporting Information), the MB removal rate only presents a minor increase compared to that containing 50 mg $g\text{-C}_3\text{N}_4$ nanosheets. This behavior is mainly caused by the more severe aggregation of the $g\text{-C}_3\text{N}_4$ nanosheets in the hybrid IPN hydrogel, which can significantly reduce the specific surface area of the $g\text{-C}_3\text{N}_4$ nanosheets. Thus, the optimized amount of $g\text{-C}_3\text{N}_4$ nanosheets in our present hybrid IPN hydrogel is 50 mg. In the present work, it enables the use as a detector being pasted on plant leaves.

In our previous investigation,^[40] hybrid IPN hydrogels presented a typical elastomer compression behavior. By comparing the compressive strength, the breaking stress of the hybrid alginate- $\text{Ca}^{2+}/\text{P}(\text{NM-co-O}_{300})/g\text{-C}_3\text{N}_4$ IPN hydrogel was slightly improved due to the introduction and homogenous dispersion of $g\text{-C}_3\text{N}_4$ nanosheets. In the present investigation, due to the presence of the additional PP fabrics, the change of tensile strength in the hybrid IPN hydrogel on the PP fabrics is also of great interest. For this reason, the breaking strengths of the pure hybrid IPN hydrogel, the PP fabrics, and the hybrid IPN hydrogel on the PP fabrics are measured (Figure 3b). The breaking stress of the pure hybrid IPN hydrogel (blue) is only 0.3 MPa, indicating that the mechanical properties of pure hydrogels are poor even with the IPN structure.

Simultaneously, the breaking stresses of the PP fabrics (orange) and the hybrid IPN hydrogel on the PP fabrics (red) are 1.4 and 1.7 MPa, respectively. Thus, it can be concluded that the mechanical properties are dramatically improved (567%) by the introduction of PP fabrics into the hybrid IPN hydrogel. Traditional hydrogels lack strength and will easily break into pieces after several cycles during use. In our present investigation, the presence of the PP fabrics enhances the strength of the

hydrogel, which is favorable for the recyclability and lifetime of the hybrid IPN hydrogels. In addition, the tensile stress–tensile strain curves of hybrid IPN hydrogels, PP fabrics, and hybrid IPN hydrogel on PP fabrics are presented in Figure S3, Supporting Information. The width of the samples is fixed as 2 cm, whereas the thicknesses of hybrid IPN hydrogels, PP fabrics, and hybrid IPN hydrogel on the PP fabrics are 1.15, 0.12, and 0.15 mm, respectively. Although the hybrid IPN hydrogels are the thickest, they present the worst mechanical properties (blue curve in Figure S3, Supporting Information). Therefore, the pure hybrid IPN hydrogels are not suitable for the desired applications. On the contrary, the PP fabrics present much better mechanical properties (black curve in Figure S3, Supporting Information). After introduction of the PP fabrics into the hybrid IPN hydrogels, the mechanical properties are significantly improved (red curve in Figure S3, Supporting Information), which is beneficial for real applications. It should be noted that the tensile stress of the hybrid IPN hydrogel on PP fabrics is lower than that of the PP fabrics in the low range of tensile strain (4–17%). This behavior might be related to the larger thickness of the hybrid IPN hydrogels on PP fabrics compared to the PP fabrics. As presented in Figure 3c, there is no prominent change of the MB removal during five repetitive cycles, which demonstrates that the hybrid IPN hydrogel on the PP fabrics possesses an excellent recyclability. In addition, the shape of the hybrid IPN hydrogel on the PP fabrics remains unchanged even after five cycles (bottom in Figure S4, Supporting Information), which is a huge advance compared to traditional hydrogels (top in Figure S4, Supporting Information). Although pure hybrid IPN hydrogels are slightly thicker, they break already (addressed by the red dashed circle) after five cycles. Thus, the easy and efficient recyclability of the photocatalyst can be realized by introducing PP fabrics into the hybrid IPN hydrogels.

2.3. Hydrogel-Based Detector to Monitor Solar Radiation Dose Required for Plant Growth

The hybrid IPN hydrogel on the PP fabrics appears to be a promising platform for lightweight solar radiation detectors. Sunshine is mimicked with the spectrum of a xenon lamp (HDL-II, Bobei

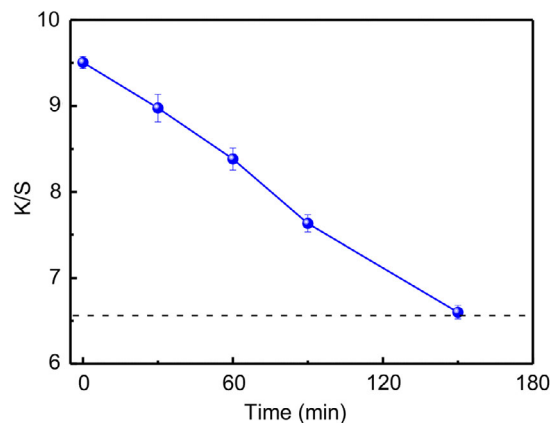


Figure 4. K/S value of the hydrogel-based detector containing 4 mg MB as a function of the exposure time to radiation from a xenon lamp.

Lighting Electrical Factory, China) and in the present study the distance between the hydrogel-based detector and the light source is fixed to 10 cm.^[40] The K/S value is applied to quantify the discoloration of the hydrogel-based detector after exposure to the xenon lamp radiation for different times. As presented in **Figure 4**, the initial K/S values of the hydrogel-based detector containing 4 mg MB and without MB are 9.5 (blue curve) and 6.6 (black dashed line), respectively. Due to the presence of MB, the K/S value is significantly larger in the hydrogel-based detector containing MB. After 150 min, MB in the hydrogel-based detector is completely degraded by $g\text{-C}_3\text{N}_4$. Notably, the K/S value decreases linearly with the radiation time, which demonstrates that the discoloration in the hydrogel-based detector is stable and can be directly observed by a simple visual inspection. Photographs of the hydrogel-based detector before and after radiation can be found in **Figure S5**, Supporting Information.

In particular, shade-tolerant plants have strict requirements to sunshine conditions such as light intensity and time.^[45,46] Although the amount of solar radiation required is limited, the shade-tolerant plants still need sunshine for survival. The chlorophyll content in shade-tolerant plants is one of the important indicators reflecting the leaves' function. As a shade-tolerant plant, *E. aureum* needs 12 h of solar radiation every week to obtain sufficient energy for growth, photosynthesis, and material metabolism. Because the sunshine intensity varies from sunrise to sunset, the solar radiation in one day is measured to precisely calculate the solar radiation dose required for *E. aureum*. The location and date for the measurement are Hangzhou, China (120.2 E, 30.3 N) and 8–18 o'clock on June 3, 2022. As shown in **Figure 5**, the light intensity from 8 to 18 o'clock is measured by the laser power meter (LP-3B, Beijing Wuke Optoelectronics Technology Co., Ltd., China). By integration, the corresponding solar radiation dose is calculated as $1.5 \times 10^7 \text{ J m}^{-2}$. Hence, the solar radiation dose required by *E. aureum* (12 h) is about $7.5 \times 10^6 \text{ J m}^{-2}$.

To fit the solar radiation dose required by *E. aureum* with those required for discoloration of hydrogel-based detector containing MB, different amounts of MB are added into the hydrogel-based detector. **Table 1** shows the radiation time and dose for the full

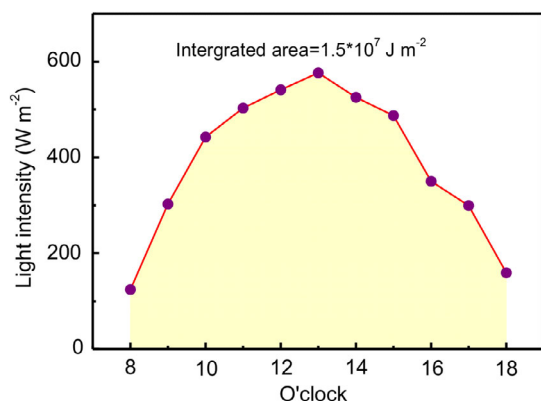


Figure 5. The static light intensity in the time frame between 8 and 18 o'clock and the corresponding solar radiation dose in Hangzhou, China (120.2 E, 30.3 N).

Table 1. Time, radiation doses, and corresponding photographs for the full discoloration of the hydrogel-based detector containing different amounts of MB.

MB quality [mg]	Time required by full discoloration [min]	Radiation dose [10^5 J m^{-2}]	Photographs before radiation	Photographs after radiation
1	33 ± 5	9.9		
2	75 ± 5	22.6		
4	140 ± 10	42.2		
8	250 ± 10	75.4		

discoloration of a hydrogel-based detector containing different amounts of MB as well as the corresponding photographs before and after radiation. When the light intensity of the xenon lamp is fixed as 503.2 W m^{-2} , the radiation time required for the full discoloration of the hydrogel-based detector containing 1, 2, 4, and 8 mg MB is 33 ± 5 , 75 ± 5 , 140 ± 5 , and 250 ± 5 min, respectively. The corresponding radiation doses are 9.9×10^5 , 2.3×10^6 , 4.2×10^6 , and $7.5 \times 10^6 \text{ J m}^{-2}$, respectively. Considering that the solar radiation dose required for the growth of *E. aureum* is $7.5 \times 10^6 \text{ J m}^{-2}$, the hydrogel-based detector containing 8 mg MB is perfectly suited to monitor the solar radiation dose required by *E. aureum* to avoid the possible burn to leaves under sunshine.

As shown in **Figure 6**, due to the low weight of the PP fabrics used as substrate and the good adhesion of the polyurethane resin used as a glue, the hydrogel-based detector can firmly adhere onto the leaves of *E. aureum* for a real outdoor measurement (Hangzhou, China (120.2 E, 30.3 N), and 11–15 o'clock on June 7, 2022). Even in case the leaves are blown by wind, the detector is still very stable fixed to the leaves. Due to the existence of both chemical and physical cross-linking, the hybrid IPN hydrogel on the PP fabrics is very stable against solar radiation. As seen in our former investigation, even after five consecutive adsorption–degradation cycles of hybrid hydrogels, no significant changes were observed in the MB adsorption and degradation.^[41] Thus, it can be concluded that the redox reactions with active species generated by $g\text{-C}_3\text{N}_4$ nanosheets do not cause any damage to the hybrid hydrogels. In addition, as shown in **Figure 6b**, only MB in the hybrid hydrogels is photodegraded by $g\text{-C}_3\text{N}_4$ nanosheets after solar radiation. Therefore, the hybrid IPN hydrogels on the PP fabrics are not photodegraded by $g\text{-C}_3\text{N}_4$



Figure 6. Photographs of the hydrogel-based detector paste on the leaves of *E. aureum* a) before and b) after solar radiation in a real outdoor scenario.

nanosheets in combination with solar radiation. To further investigate the stability of the hydrogel-based detector, the control sample is further investigated in the dark environment. The hydrogel-based detector is placed in the dark for 0, 12, and 24 h, respectively. As shown in Figure S6, Supporting Information, in the dark environment, the hydrogel-based detector basically remains unchanged with time, which confirms the stability of the hydrogel-based detector. An infrared thermal imager (FLTR E4, FLIR Systems, Inc., USA) is applied to measure the temperature of the hydrogel-based detector on the leaves of *E. aureum* before and after light irradiation. As shown in Figure S7a, Supporting Information, the infrared thermal image shows a temperature of the hydrogel-based detector on the leaves of *E. aureum* before light irradiation of 25.8 °C. After light irradiation for 0.5 (Figure S7b, Supporting Information), 1.0 (Figure S7c, Supporting Information), and 1.5 h (Figure S7d, Supporting Information), the temperature varies between 24.0 and 25.6 °C. Thus, the temperature basically remains unchanged. It can be concluded that the g-C₃N₄ nanosheets possess no photothermal heating effect during light radiation and will not affect the plants during light radiation. Moreover, the water retention of the hydrogel-based detector is also measured. As shown in Table S1, Supporting Information, the weights of the hydrogel-based detector in the dry and swollen states are 0.23 and 1.47 g, respectively. Therefore, the water retention of the swollen hydrogel-based detector is 84%. When placed in ambient conditions, the hydrogel indeed gradually loses water with time. However, the discoloration time is only 4 h for the presented hydrogel-based detector and the hydrogel-based detector only needs to remain hydrated in this limited period. According to the photographs presented in Figure 6b, the hydrogel-based detector is still hydrated and stable after solar radiation. It should be noted that the detector can be easily removed after use without any damage to the leaves. As shown in Figure S8, Supporting Information, the full discoloration of the hydrogel-based detector containing 8 mg MB requires 4 h of solar radiation (from 11 to 15 o'clock). The corresponding solar radiation dose is $6.4 \times 10^6 \text{ J m}^{-2}$, which is very close to the theoretical value ($7.5 \times 10^6 \text{ J m}^{-2}$) required for the growth of *E. aureum*. It can be concluded that the thin layer of polyurethane resin does not influence the discoloration of the hydrogel-based detector. Due to the high viscosity, the

hydrophilic polyurethane resin plays the role of glue in our present investigation.

Based on the above discussion, it can be concluded that the present hydrogel-based detector containing MB is very suitable for monitoring a solar radiation dose to ensure the sufficient radiation for plant growth and avoid possible burn by tracing the discoloration.

3. Conclusion

Solar radiation exposed to plant leaves can be accurately traced by the hybrid alginate-Ca²⁺/P(NM-co-O₃₀₀)/g-C₃N₄ IPN hydrogel-based detector. By introducing PP fabrics as supporting substrates, the thickness and weight of the hybrid hydrogels are significantly reduced, which enables lightweight detectors. Moreover, the photodegradation performance of MB is profoundly increased due to the larger surface area. The hybrid IPN hydrogel on the PP fabrics with a thickness of 1.5 mm can remove more than 95% of MB from an aqueous MB solution (200 mL, 10 mg L⁻¹) in less than 3 h under visible light radiation. In combination with the advantage of a good adhesion introduced by using a polyurethane resin as glue, the obtained hydrogel-based detector can be easily pasted on the leaves of plants. We demonstrate this usage with the example of *E. aureum* to monitor the solar radiation dose by simply checking the extent of discoloration. The use of such on plant detector can significantly avoid a possible burn of the plant leaves due to an overexposure to sunshine. To extend the use of the detector to other plants, only the amount of MB needs to be adjusted. Thereby, the developed hybrid IPN hydrogel on the PP fabrics presents an optimal platform for lightweight solar radiation detectors.

4. Experimental Section

Materials: Sodium alginate salt (SA, AR), calcium chloride (CaCl₂, AR), and oligo(ethylene glycol) methyl ether methacrylate (O₃₀₀, purity 95%) were purchased from Sigma-Aldrich. N-isopropylacrylamide (NM, purity 98%), N,N'-methylenebisacrylamide (MBA, purity 99%), and MB (AR) were bought from Macklin. Triethylamine (AR) was from Wuxi Zhanwang Chemical Reagent Co., Ltd. PP fabrics with a thickness of 0.2 mm and dicyandiamide (AR) were purchased from Sinopharm Chemical Reagent Co., Ltd. The hydrophilic polyurethane resin (HX-W910L) was obtained from Zhejiang Hexin Science and

Technology Co., Ltd. Before polymerization, NIPAM was purified as follows: NIPAM (0.08 mol, 9 g) was first added to 200 mL *n*-hexane. Then the solution was moved into a water bath thermostated at 50 °C to realize full dissolution. After filtering, the filtrate was recrystallized at 4 °C.

Synthesis of *g*-C₃N₄ Nanosheets: The synthesis of *g*-C₃N₄ can be found in our previous publication.^[40] Bulk *g*-C₃N₄ was prepared by thermally decomposing dicyandiamide at 550 °C for 4 h in a static air atmosphere with a ramp rate is 5 °C min⁻¹. Then the bulk *g*-C₃N₄ was ground into powder and thermostated at 520 °C for 2 h with a ramping rate of 2 °C min⁻¹. Based on the protocol mentioned above, *g*-C₃N₄ with a yellow nanosheets structure can be obtained.

Preparation of the Solar Radiation Detector: Based on the initiation mechanism of *g*-C₃N₄ nanosheets,^[40,47] *g*-C₃N₄ nanosheets and triethylamine were applied to co-initiate the polymerization of the hybrid IPN hydrogel on the PP fabrics under UV radiation. The UV light with a wavelength of 365 nm (power of 3 W) was selected as the source to obtain a high and suitable initiating quantum yield.

The preparation of the solar radiation detector was as follows: MB with different quality, SA (0.46 mol, 0.1 g), NM (5 mmol, 0.5 g), MBA (0.07 mmol, 0.0135 g), O₃₀₀ (5 mmol, 0.714 mL), and *g*-C₃N₄ (0.5 mmol, 50 mg) were added into deionized water (10 mL). After stirring for 120 min, 90 μL triethylamine was added to the homogeneously mixed solution and then the mixture was transferred into a glass dish containing PP fabrics with a diameter of 4 cm. The mixture in a glass dish was radiated by a UV light for 2 h at 50 °C. Afterward, it was solidified for 12 h at room temperature. To realize the physical cross-linking of Ca²⁺, the obtained hybrid hydrogels were immersed in 50 mL CaCl₂ solution with a concentration of 10 g L⁻¹ for 1 h. Finally, the hybrid IPN hydrogel on the PP fabrics was immersed in the hydrophilic polyurethane resin to obtain the final solar radiation detector. The hydrophilic polyurethane resin plays the role of glue based on its viscose property. A thin polyurethane resin layer can be formed on the surface of the hydrogel-based detector after being immersed in a hydrophilic polyurethane resin. Thus, the hydrogel-based detector can firmly adhere onto the leaves of *E. aureum* for a real outdoor measurement. Moreover, this polyurethane resin shell does not influence the discoloration of the hydrogel-based detector. Notably, the preparation of hybrid alginate-Ca²⁺/P(NM-co-O₃₀₀)/*g*-C₃N₄ IPN hydrogel on the PP fabrics co-initiated by *g*-C₃N₄ and triethylamine is similar to the above-described preparation method without MB and the hydrophilic polyurethane resin. In our present investigation, a glass dish is used as container for the preparation of the hybrid hydrogel-based detector. Because the amount of each component in the hybrid IPN hydrogels on the PP fabrics remains unchanged during preparation, its thickness can be simply controlled by changing the diameter of the container. The mixed solution for the preparation of the hydrogel was transferred into the glass dish with a diameter of 4, 6, and 8 cm, respectively. After 2 h of UV radiation at 50 °C, the thicknesses of the obtained hybrid IPN hydrogels on the PP fabrics are about 6.0, 3.0, and 1.5 mm, respectively.

ATR-FTIR Spectroscopy: ATR-FTIR spectroscopy (Vertex 70 spectrometer, Bruker, USA) was applied to investigate the functional groups on PP fabrics, *g*-C₃N₄ nanosheets, and hybrid IPN hydrogels on PP fabrics. The range of the scanning wavenumber was from 600 to 4000 cm⁻¹.

Electron Microscopy Measurements: Field emission scanning electron microscopy (FE-SEM) (ULTRA55, Carl Zeiss SMT Pte Ltd., UK) was used to observe the morphology of the original PP fabrics and hybrid IPN hydrogels on PP fabrics. The accelerating voltage and distance applied in the measurement were 3 kV and 8 mm, respectively. Before the measurements, the samples were sputter-coated with platinum by an auto-fine coater (JEOL, JFC-1600).

TEM (JEM-2100, JEOL, Japan) was applied to probe the distribution of *g*-C₃N₄ in the hybrid IPN hydrogels on PP fabrics. The accelerating voltage applied in the measurements was 150 kV. Before measurements, the embedded sectioning technique (UC7, Leica, Germany) was applied to prepare the samples because the hybrid IPN hydrogels on PP fabrics were bulk materials.

Mechanical Strength Measurements: The electronic universal material tester (Instron 3367, American Instron Company) was used to measure the breaking strength of the hybrid IPN hydrogels and PP fabrics as well

as of the hybrid IPN hydrogels on PP fabrics (4 × 2 cm²). In our present investigation, the thickness of hybrid IPN hydrogels and hybrid IPN hydrogels on PP fabrics remains unchanged (1.5 mm) during the mechanical strength measurements.

Dye Removal Measurements: During the measurements, hybrid IPN hydrogel on the PP fabrics were used to remove MB from the aqueous solution (10 mg L⁻¹, 200 mL). The LED light band (length of 1 m, containing 120 white light beads) was used to simulate the solar light. The total power and luminous flux of the LED lights were 13 W and 1300 lm, respectively. The UV spectrophotometer (Perkin Elmer, UV-vis Lambda 35) was applied to probe the change of MB in the aqueous solution after different exposure times.

To further investigate the stability of the hybrid IPN hydrogel on the PP fabrics, the dye removal measurement was repeated for five cycles in the hybrid IPN hydrogel on the PP fabrics (thickness of 1.5 mm). Light exposure time is set to 5 h for each cycle because all MB can be removed from an aqueous solution by the hybrid IPN hydrogel on the PP fabrics in this period.

Discoloration Measurements of the Solar Radiation Detector: Because the spectrum of the xenon lamp is very similar to that of the sunshine, the xenon lamp is greatly favorable for a sunshine simulation and the distance between the solar radiation detectors with the light source was set to 10 cm. The laser power meter (LP-3B, Beijing Wuke Optoelectronics Technology Co., Ltd., China) was applied to measure the light intensity. The light intensity was 503.2 W m⁻² at this distance, which is extremely close to the real intensity of sunshine. Under xenon lamp (HDL-II, Bobei Lighting Electrical Factory, China) radiation at different times, the color measuring and matching instrument (DC 600, Datacolor Company, USA) was applied to quantify the discoloration of the solar radiation detector. Dyeing depth is one of the important indicators for evaluating the dyeing performance. It can be defined by the Kubelka–Munk dyeing depth equation. In this equation, *K* and *S* are the absorption and scattering coefficients of the measured sample, respectively.^[48,49] Based on the relationship between *K*, *S*, and concentration (*C*) of dyes in the Kubelka–Munk dyeing depth equation, a larger *K/S* value indicates a higher concentration of the dye. Thus, the *K/S* value can be used to quantify the residual amount of dyes in the hydrogel-based detector during the discoloration process.

Supporting Information

Supporting Information is available from the Wiley Online Library or from the author.

Acknowledgements

This work was supported by the Fundamental Research Funds of Zhejiang Sci-Tech University (grant no. 2021Y003). P.M.-B. acknowledges support by TUM.solar in the context of the Bavarian Collaborative Research Project Solar Technologies Go Hybrid (SolTech).

Open Access funding enabled and organized by Projekt DEAL.

Conflict of Interest

The authors declare no conflict of interest.

Data Availability Statement

The data that support the findings of this study are available from the corresponding author upon reasonable request.

Keywords

Epipremnum aureum, graphitic carbon nitride, hybrid hydrogels, polypropylene fabrics, solar radiation detector

Received: August 1, 2022

Revised: September 12, 2022

Published online: September 29, 2022

- [1] Z. P. Xing, P. Wu, M. Zhu, H. J. Qian, Y. J. Hu, B. W. Guo, H. Y. Wei, K. Xu, Z. Y. Huo, Q. G. Dai, H. C. Zhang, *China, J. Integr. Agric.* **2017**, *16*, 1923.
- [2] N. Y. Deng, X. X. Ling, Y. Sun, C. D. Zhang, S. Fahad, S. B. Peng, K. H. Cui, L. X. Nie, J. L. Huang, *Eur. J. Agron.* **2015**, *64*, 37.
- [3] R. G. Alderfer, *Sol. Energy* **1973**, *15*, 77.
- [4] J. L. Gong, Z. P. Xing, Y. J. Hu, H. C. Zhang, Q. G. Dai, Z. Y. Huo, K. Xu, H. Y. Wei, H. Gao, *Chinese J. Rice Sci.* **2014**, *28*, 267.
- [5] C. R. Brodersen, T. C. Vogelmann, W. E. Williams, H. L. Gorton, *Plant Cell Environ.* **2008**, *31*, 159.
- [6] S. Kataria, S. S. Baroniya, L. Baghel, M. Kanungo, *Plant Sci. Today* **2014**, *1*, 224.
- [7] M. L. Bianculli, L. A. N. Aguirrezábal, G. A. P. Irujo, M. M. Echarte, *Eur. J. Agron.* **2016**, *77*, 1.
- [8] E. Brugnoli, M. Lauteri, *Plant Physiol.* **1991**, *95*, 628.
- [9] F. Gao, V. Catalayud, E. Paoletti, Y. Hoshika, Z. Z. Feng, *Environ. Pollut.* **2017**, *230*, 268.
- [10] M. R. Ismail, S. W. Burrage, H. Tarmizi, M. A. Aziz, *Sci. Hortic.* **1994**, *60*, 101.
- [11] A. Coffey, M. A. K. Jansen, *Plant Physiol. Biochem.* **2019**, *134*, 64.
- [12] D. Verdager, M. A. K. Jansen, L. Llorens, L. O. Morales, S. Neugart, *Plant Sci.* **2017**, *255*, 72.
- [13] A. Kume, *J. Plant Res.* **2017**, *130*, 501.
- [14] M. M. Caldwell, L. O. Björn, J. F. Bornman, S. D. Flint, G. Kulandaivelu, A. H. Teramura, M. Tevinie, *J. Photochem. Photobiol. B* **1998**, *46*, 40.
- [15] R. Podolec, E. Demarsy, R. Ulm, *Annu. Rev. Plant Biol.* **2021**, *72*, 793.
- [16] S. Li, Y. H. Tian, K. Wu, Y. F. Ye, J. P. Yu, J. Q. Zhang, Q. Liu, M. Y. Hu, H. Li, Y. P. Tong, N. P. Harberd, X. D. Fu, *Nature* **2018**, *560*, 595.
- [17] L. Y. Lan, J. Q. Xiong, D. Gao, Y. Li, J. Chen, J. Lv, J. F. Ping, Y. B. Ying, P. S. Lee, *ACS Nano* **2021**, *15*, 5307.
- [18] E. H. Pritchard, R. H. Simons, *Lighting Res. Technol.* **1992**, *24*, 107.
- [19] S. Ye, R. Wang, M. Z. Wu, Y. P. Yuan, *Appl. Surf. Sci.* **2015**, *358*, 15.
- [20] S. C. Yan, Z. S. Li, Z. G. Zou, *Langmuir* **2009**, *25*, 10397.
- [21] S. C. Yan, Z. S. Li, Z. G. Zou, *Langmuir* **2010**, *26*, 3894.
- [22] M. Groenewolt, M. Antonietti, *Adv. Mater.* **2005**, *17*, 1789.
- [23] K. Wang, Q. Li, B. Liu, B. Cheng, W. Ho, J. Yu, *Appl. Catal. B: Environ.* **2015**, *176–177*, 44.
- [24] Y. Chen, W. Huang, D. He, Y. Situ, H. Huang, *ACS Appl. Mater. Interfaces* **2014**, *6*, 14405.
- [25] M. Xiao, B. Luo, S. Wang, L. Wang, *J. Energy Chem.* **2018**, *27*, 1111.
- [26] F. Dong, Z. W. Zhao, T. Xiong, Z. L. Ni, W. D. Zhang, Y. J. Sun, W. K. Ho, *ACS Appl. Mater. Interfaces* **2013**, *5*, 11392.
- [27] F. Brandl, M. Henke, S. Rothschenk, R. Gschwind, M. Breunig, T. Blunk, J. Tessmar, A. Göpferich, *Adv. Eng. Mater.* **2007**, *9*, 1141.
- [28] N. A. Peppas, J. J. Sahlin, *Biomaterials* **1996**, *17*, 1553.
- [29] E. A. Kamoun, X. Chen, M. S. Mohy Eldin, E. R. S. Kenawy, *Arab. J. Chem.* **2015**, *8*, 1.
- [30] J. F. Mano, *Adv. Eng. Mater.* **2008**, *10*, 515.
- [31] K. Y. Lee, D. J. Mooney, *Chem. Rev.* **2001**, *101*, 1869.
- [32] Z. Zhang, F. Xiao, Y. Guo, S. Wang, Y. Liu, *ACS Appl. Mater. Interfaces* **2013**, *5*, 2227.
- [33] P. Gu, N. Fan, Y. X. Wang, J. P. Wang, P. Müller-Buschbaum, Q. Zhong, *ACS Appl. Mater. Interfaces* **2019**, *11*, 30269.
- [34] L. Lei, W. J. Wang, C. Wang, H. Q. Fan, A. K. Yadav, N. Hu, Q. Zhong, P. Müller-Buschbaum, *J. Mater. Chem. A* **2020**, *8*, 23812.
- [35] X. F. Zhang, T. T. Li, Q. Jiang, L. W. Wu, H. T. Ren, H. K. Peng, B. C. Shiu, Y. T. Wang, C. W. Lou, J. H. Lin, *Prog. Org. Coat.* **2020**, *149*, 105919.
- [36] J. H. Kim, S. B. Lee, S. J. Kim, *Polymer* **2002**, *43*, 7549.
- [37] A. A. AL Kahtani, B. S. Sherigara, *Colloids Surf., B* **2014**, *115*, 132.
- [38] X. Zhang, R. Zhuo, *J. Colloid. Interface Sci.* **2000**, *223*, 311.
- [39] Z. P. Du, X. F. Sun, X. M. Tai, G. Y. Wang, X. Y. Liu, *RSC Adv.* **2015**, *5*, 17194.
- [40] N. Hu, L. Lin, J. Tan, W. J. Wang, L. Lei, H. Q. Fan, J. P. Wang, P. Müller-Buschbaum, Q. Zhong, *ACS Appl. Mater. Interfaces* **2020**, *12*, 56480.
- [41] N. Hu, C. Chen, J. Tan, W. J. Wang, C. Wang, H. Q. Fan, J. P. Wang, P. Müller-Buschbaum, Q. Zhong, *ACS Appl. Polym. Mater.* **2020**, *2*, 3674.
- [42] X. Y. Song, S. Z. Zhou, Y. F. Wang, W. M. Kang, B. W. Cheng, *Fibers Polym.* **2012**, *13*, 1015.
- [43] Y. Q. Li, Z. B. Xia, Q. Gong, X. H. Liu, Y. Yang, C. Chen, C. H. Qian, *Synth. Met.* **2021**, *280*, 116891.
- [44] G. Y. Feng, X. Y. Wang, D. T. Zhang, H. J. Cao, K. Qian, X. L. Xiao, *Constr. Build. Mater.* **2017**, *157*, 372.
- [45] G. H. Krause, K. Winter, S. Matsubara, B. Krause, P. Jahns, A. Virgo, J. Aranda, M. García, *Photosynth. Res.* **2012**, *113*, 273.
- [46] G. H. Krause, E. Grube, A. Virgo, K. Winter, *Plant Physiol.* **2003**, *131*, 745.
- [47] J. Liu, T. An, Z. Chen, Z. Wang, H. Zhou, T. Fan, D. Zhang, M. Antonietti, *J. Mater. Chem. A* **2017**, *5*, 8933.
- [48] T. R. Bai, K. Kobayashi, K. Tamura, Y. Jun, L. J. Zheng, *J. CO2 Util.* **2019**, *33*, 253.
- [49] W. Y. Wang, J. C. Chiou, W. X. Chen, J. L. Yu, C. W. Kan, *Cellulose* **2021**, *28*, 6651.